

## Coordination Chemistry

Photoisomerization of Bis(tridentate) 2,6-Bis(1*H*-pyrazol-1-yl)pyridine Ligands Exhibiting a Multi-anthracene SkeletonIvan Šalitroš,<sup>\*,[a, b]</sup> Olaf Fuhr,<sup>[a, c]</sup> Miroslav Gál,<sup>[b]</sup> Michal Valášek,<sup>[a]</sup> and Mario Ruben<sup>\*,[a, d]</sup>

**Abstract:** A novel molecular design is described where two peripheral moieties made of 2,6-bis(1*H*-pyrazol-1-yl)pyridine are linked through multi-1,8-diethynylantracene moieties. The optimized synthesis of the three isostructural analogues **1 a**, **1 b**, and **1 c**, containing the anthraquinone, anthracene, and 10-methoxyanthracene units, respectively, is reported. The resulting spatial face-to-face arrangement of the peripheral anthracene rings enables to trigger the intramolecular

[4+4] photocycloaddition affording the isomers **P1 b** and **P1 c**, which can be thermally cleaved back to the original anthracene derivatives **1 b** and **1 c**, respectively. Single-crystal X-ray diffraction studies confirm the expected molecular structures of compounds **1 a–1 c** as well as of their corresponding isomers **P1 b** and **P1 c**. The spectral, optical, and electrochemical properties of all synthesized compounds are investigated and discussed.

## Introduction

The design, development, and study of molecular materials with tailored physical properties are the ultimate goal for current synthetic chemistry.<sup>[1–4]</sup> Among a wide range of systems under investigation, coordination materials that exhibit switching between two or more distinct magnetic states have received considerable interest for both their fundamental behavior as well as for the application of future memory or display devices.<sup>[5–8]</sup> Special attention has been focused on complexes with phototunable magnetic properties, where, by using light as cheap and convenient trigger, it becomes possible to directly alter the various magnetic states of a metal center.<sup>[9]</sup> In the vast majority of examples, however, the existence of photoexcited metastable states is observed up to cryogenic temperatures only.<sup>[10]</sup> On the other hand, alternative light-induced changes created in the ligand environment might influence

the magnetic states of the central atoms as well. Indeed, so far, several examples of coordination compounds were reported, in which photoisomerizable ligands, that is, stilbenes<sup>[11,12]</sup> or azobenzenes,<sup>[13]</sup> control the spin state of a metal center under isothermal conditions. Moreover, reversible photoisomerization of ligands works under ambient conditions and so light-induced spin-state switching can be achieved even at room temperature.<sup>[14,15]</sup> Throughout the search for molecular systems exhibiting ligand-driven light-induced magnetic switching, to the best to our knowledge, there is only one coordination compound reported so far that employs the photoisomerizable properties of anthracene units.<sup>[16]</sup> In comparison, a multitude of [4+4] photocycloaddition reactions has been reported for multi-anthracene organic materials (i.e., refs. [17–19]). Visible-light photocyclization of two neighboring anthracene moieties, high thermal stability of the photoproducts, and easy thermal or photocycloreversion are characteristic features of such organic systems.<sup>[20–22]</sup> The unique shape and the aromatic character of anthracene derivatives allows to synthesize molecules with a regular molecular architecture<sup>[23,24]</sup> and/or with specific supramolecular arrangements in the crystal lattice, thereby supporting the light-induced isomerization, dimerization, or polymerization in the solid state.<sup>[25,26]</sup> Moreover, Schlüter et al. and King et al. recently achieved a single-crystal-to-single-crystal photopolymerization and subsequent exfoliation of structurally characterized 2D polymers.<sup>[27,28]</sup> Such results highlight the potential of polycondensed anthracene molecular building blocks for the creation of functionalized polymers as alternative carbon allotropes.

Our goal was to design photoisomerizable multi-anthracene systems in combination with N-donor moieties, which will allow to 1) coordinate transition metals and 2) form oligomeric structures, exhibiting a regular molecular architecture. In this sense, 2,6-bis(1*H*-pyrazol-1-yl)pyridine (bpp) derivatives represent a promising ter-dentate ligand system that, when coordi-

[a] Prof. I. Šalitroš, Dr. O. Fuhr, Dr. M. Valášek, Prof. M. Ruben  
Institute of Nanotechnology, Karlsruhe Institute of Technology (KIT)  
Hermann-von-Helmholtz-Platz 1  
76344, Eggenstein-Leopoldshafen (Germany)  
E-mail: mario.ruben@kit.edu

[b] Prof. I. Šalitroš, Prof. M. Gál  
Department of Inorganic Chemistry  
Faculty of Chemical and Food Technology  
Slovak University of Technology, Bratislava, 81237 (Slovak Republic)  
E-mail: ivan.salitros@stuba.sk

[c] Dr. O. Fuhr  
Karlsruhe Nano-Micro Facility (KNMF)  
Karlsruhe Institute of Technology (KIT), Hermann-von-Helmholtz-Platz 1  
76344 Eggenstein-Leopoldshafen (Germany)

[d] Prof. M. Ruben  
Institut de Physique et Chimie des Matériaux de Strasbourg (IPCMS)  
CNRS-Université de Strasbourg, 23 rue du Loess, BP 43  
67034 Strasbourg cedex 2 (France)

Supporting information for this article can be found under:  
<https://doi.org/10.1002/chem.201700825>.

nated by iron(II) atoms, gives access to thermally and photoinduced spin-crossover bistability<sup>[29,30]</sup> often accompanied by thermal hysteresis loops around room temperature.<sup>[31–34]</sup> Herein, we propose a photoactive skeleton consisting of two peripheral anthracene-bpp moieties connected on various central aromatic units (Figure 1). Here, we will present the target-directed synthesis of the bis(tridentate) organic ligands **1a**, **1b**, and **1c** in detail. The intramolecular [4+4] photocyclization of compounds **1a–1c** in solution afforded the compounds **P1b** and **P1c**, which could be back-converted to their native isomers **1b** and **1c** by thermal decyclization (Figure 1). The synthesized ligands and related photoisomers have been structurally characterized and their spectral, optical, and electrochemical properties were investigated in detail.

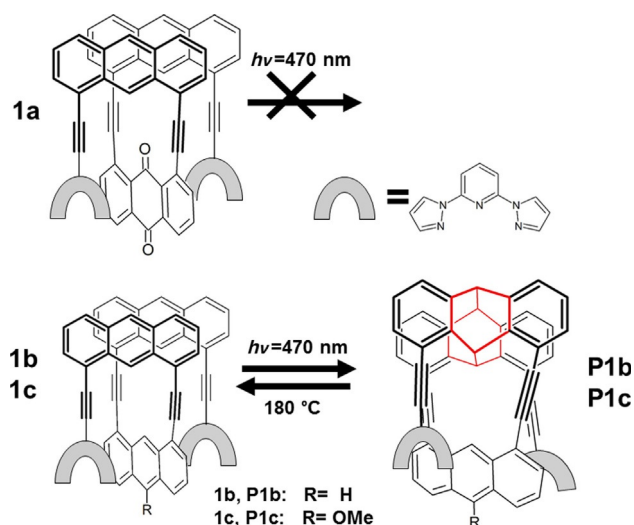


**Figure 1.** Molecular structures of the reported compounds and their ability of [4+4] photoisomerization.

## Experimental Section

### Equipment, measurements, and materials

All NMR spectra were recorded on a Bruker Avance 500 spectrometer at 25 °C in [D<sub>6</sub>]DMSO, CD<sub>2</sub>Cl<sub>2</sub>, or CDCl<sub>3</sub> and referenced to the solvent residual signal. Electrospray ionization time-of-flight (ESI-TOF) mass spectrometric analytical data were acquired on a Bruker microTOF QII mass spectrometer. Elemental analyses were obtained by using a Vario Micro Cube CHNS analyzer. IR spectra were recorded with a Perkin–Elmer GX FTIR spectrometer in KBr pellets or by ATR technique in the range of  $\tilde{\nu}$  = 4000–400 cm<sup>-1</sup> with a Nicolet Magna FTIR 750 spectrometer. UV/Vis spectra were recorded with a Varian Cary 500 Scan spectrophotometer in a 1 cm quartz cell at ambient temperature (extinction coefficients are given below in units of Lmol<sup>-1</sup>cm<sup>-1</sup>). Fluorescence spectra were measured with a Varian Cary Eclipse Fluorescence spectrometer at room temperature in a 1 cm quartz cell. All reagents (sodium anthraquinone-1-sulfonate, nitric acid, sulfuric acid, sodium chlorate, hydrochloric acid, sodium sulfide nonahydrate, sodium nitrite, potassium iodide, sodium borohydride, (triisopropylsilyl)acetylene (TIPSA), tetrakis(triphenylphosphine) palladium(0), copper(I) iodide, ethynyltrimethylsilane (TMSA), nickel(II) acetylacetonate, triphenylphosphine, caesium carbonate, *n*-tetrabutylammonium fluoride tri-

hydrate, and *n*-tetrabutylammonium hexafluorophosphate) and solvents (isopropanol, methanol, *n*-hexane, and dichloromethane) were obtained from commercial suppliers and used without further purification. Tetrahydrofuran (THF) was dried over sodium/benzophenone, diisopropylamine (DIPA) was dried over CaH<sub>2</sub>, and both solvents were distilled under an argon atmosphere prior to use. Acetonitrile was dried over activated molecular sieves. Column chromatography was performed on silica gel 60 (0.040–0.063 mm, Merck). 1,8-Diiodo-9,10-anthraquinone,<sup>[35]</sup> 1,8-diiodoanthracene,<sup>[35]</sup> 1,8-diiodo-10-methoxyanthracene,<sup>[35]</sup> 1-amino-8-chloro-9,10-anthraquinone,<sup>[36]</sup> and 4-iodo-2,6-di(1*H*-pyrazol-1-yl)pyridine<sup>[32,37]</sup> were prepared as reported previously.

### Thermal decyclization experiments

The thermal decyclization of compounds **P1b** and **P1c** was investigated both in solution ([D<sub>6</sub>]DMSO) and in the solid state. The starting material (≈ 4 mg) was dissolved in anhydrous [D<sub>6</sub>]DMSO (0.6 mL), subsequently purged with argon gas, filled into an NMR tube, and heated to the desired temperature in an oil bath. The progress of the decyclization reaction was monitored by NMR spectroscopy every 60 min. In the case of the decyclization **P1b** → **1b**, no significant progress of the decyclization has been observed up to 160 °C (Figure S13 in the Supporting Information). After 1 h at 165 °C the decyclization started and after 6 h of heating at this temperature the anthracene compound **1b** was observed as the major product in the solution. After 90 min of heating at 185 °C, the conversion of compound **P1b** to compound **1b** was quantitatively. The thermal decyclization of compound **P1c** proceeded similarly and after 2 h of heating at 180 °C the major part of the cyclized material **P1b** was converted to the anthracene compound **1c** (Figure S14 in the Supporting Information). The solid-state thermal decyclization of compounds **P1b** and **P1c** was investigated as well. A glass vial was charged with the corresponding compound **P1b** or **P1c**, purged with argon gas, and sealed. A glass vial was subsequently heated up to 185 °C and kept at this temperature for two days (compound **P1b**) or three days (compound **P1c**). The progress of the annealing reactions was monitored by NMR spectroscopy (Figures S13 and S14 in the Supporting Information) and showed quantitative decyclization in both cases.

### X-ray crystallography

Single-crystal X-ray diffraction data were collected on a STOE IPDS II or IPDS2T diffractometer with graphite-monochromated Mo<sub>Kα</sub> radiation ( $\lambda$  = 0.71073 Å). The crystal was kept at 180.2 K during data collection. By using Olex2,<sup>[38]</sup> the structure was solved with the ShelXS<sup>[39]</sup> structure solution program by using direct methods and refined with the ShelXL<sup>[40]</sup> refinement package by using least squares minimization. Refinement was performed with anisotropic temperature factors for all non-hydrogen atoms (disordered atoms and atoms of non-coordinating solvent molecules were refined isotropically).

CCDC 1461800 (**1a**), 1461801 (**1b**), 1461802 (**1c**), 1461803 (**P1b**), and 1461804 (**P1c**) contain the supplementary crystallographic data for this paper. These data are provided free of charge by The Cambridge Crystallographic Data Centre.

### Electrochemistry

Electrochemical measurements were performed by using an AUTO-LAB instrument PGSTAT 302N (Metrohm). The electrochemical data from the cyclic voltammetry measurements were analyzed by using the AUTOLAB software. A three-electrode electrochemical

cell was used. The reference electrode (RE), Ag|AgCl|1 M LiCl, was separated from the test solution by a salt bridge. The working electrode (WE) was a Pt disk ( $d=2$  mm). The auxiliary electrode was a platinum net. The scan rate for the cyclic voltammetry was in the range 32–512 mV s<sup>-1</sup>. Oxygen was removed from the solution by passing a stream of argon saturated with vapors of the solvent.

## Results and Discussion

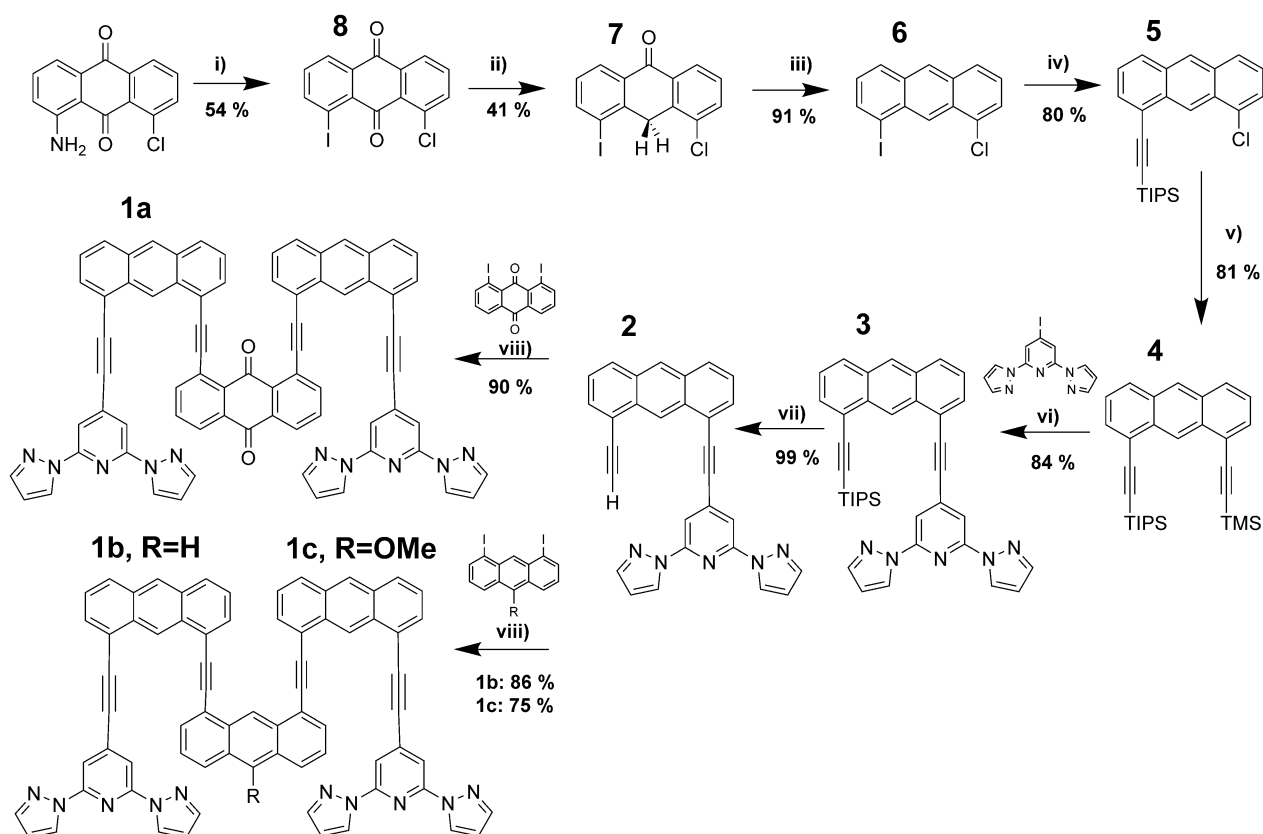
### Molecular design, synthesis, [4+4] photocycloaddition, and thermal decyclization

The coordination ability of N-donor terpyridine-like moieties is known and up to date numerous examples of mono- and polynuclear coordination systems involving this type of tridentate meridional ligands were reported.<sup>[41,42]</sup> Among them, the 2,6-bis(pyrazol-1-yl)pyridine (bpp) ligands, in particular coordinated with iron(II) metal centers, acquire an outstanding position due to the emergence of spin-crossover molecular bistability at room temperature.<sup>[31]</sup> With respect to this, our effort has been focused on the construction of systems, which incorporate two or more bpp ligand centers introduced on a photosensitive polyaromatic skeleton. Such ligands would be able to coordinate metal ions, yielding oligomeric structures in well-defined molecular architectures. The inspiration for this molecular design has been drawn by previously reported bis(tridentate) ligands, that is, 6,6'-pyrimidine-4,6-diylbis(2,2'-bipyridine),<sup>[43,44]</sup> 2-phenyl-4,5-bis[6-(3,5-dimethyl-1*H*-pyrazol-1-yl)pyrid-2-yl]-1*H*-imidazole,<sup>[45]</sup> or bis(2-(1*H*-imidazol-2-yl)-6-(pyrazol-1-yl)pyridine)-benzo[1,2-d:4,5-d']diimidazole,<sup>[46]</sup> where both neighboring N<sub>3</sub>-donor coordination embraces are aligned within the conjugated aromatic skeleton. Subsequent coordination with metal ions results in to the formation of self-assembled tetranuclear [2+2] grid complexes. Based on this, 1,8-disubstituted anthracene building blocks have been considered as a promising polyaromatic backbone for the introduction of bpp ligand moieties. In addition, the known photochemical and emission properties of condensed aromatic systems encouraged us to involve two or more anthracene moieties investigating by this way the interplay of physical properties of the metal centers and the anthracene organic skeleton of the novel ligands. Thus, we propose to create organic ligands consisting of two peripheral 4-[(8-ethynylanthracen-1-yl)ethynyl]-2,6-bis(1*H*-pyrazol-1-yl)pyridine (**2**) blocks connected to the central anthracene or anthraquinone rings in 1'- and 8'-positions and through acetylene bonds (Figure 1). The strategy of the considered synthesis is based on the formation of 1-chloro-8-iodoanthracene (**6**), which allows the selective introduction of the acetylene bonds with different protection groups. The synthesis protocol (Scheme 1) departs from the known 1-amino-8-chloroanthraquinone,<sup>[36]</sup> which was used for the conversion to 1-chloro-8-iodoanthraquinone (**8**) through a Sandmeyer reaction in concentrated sulfuric acid at 0 °C in 54% yield. The obtained anthraquinone **8** was reduced to 1-chloro-8-iodoanthracene (**6**) in a methanol suspension in two steps by using sodium borohydride. The first step of the reduction afforded the anthrone **7** in 41% yield, which was further reduced under the same conditions to the desired 1,8-disubstituted anthracene **6**. The over-

all yield of the two-step reduction was about 37%, which is comparable to the previously reported reduction of 1,8-dioanthraquinone.<sup>[47]</sup> Selective Sonogashira coupling of compound **6** and TIPSA in DIPA afforded compound **5**, which was reacted with the Grignard reagent of TMSA resulting in the formation of the TIPS- and TMS-protected 1,8-diacetyleneanthracene adduct **4** in 80% overall yield. After in-situ deprotection of TMS by cesium carbonate, 4-iodo-2,6-bis(pyrazole-1-yl)pyridine<sup>[32,37]</sup> was used for the introduction of the bpp ligand moiety onto the 1,8-diacetyleneanthracene skeleton by Sonogashira coupling in 84% yield. Next, the deprotection of the TIPS groups by TIBAF afforded 4-[(8-ethynylanthracen-1-yl)ethynyl]-2,6-bis(pyrazol-1-yl)pyridine (**2**), which was used as precursor for the formation of the ligands **1a**, **1b**, and **1c** formed after two-fold intermolecular Sonogashira coupling between compound **2** and the corresponding 1,8-diodoanthraquinone (**1a**), 1,8-diodoanthracene (**1b**), or 1,8-diodo-10-methoxyanthracene (**1c**) in a 2.2:1 ratio in THF/DIPA solution at elevated temperatures. The overall yield varies in the range of only 8–9%, which is considered to be reasonable given to the complexity of the synthetic protocol. Finally, despite of the low yields, the ligands **1a**, **1b**, and **1c** could be obtained in a scale of hundreds of milligrams.

The [4+4] photocyclization experiments were performed under blue-light irradiation ( $\lambda=(470\pm 50)$  nm) in dichloromethane solution at 5 °C as well as on single crystals. The irradiation of the anthraquinone-free ligands **1b** and **1c** afforded compounds **P1b** and **P1c** as photoisomers. Despite to the possible light-induced intermolecular dimerization or polymerization, the intramolecular isomerization took exclusively and quantitatively place. On the other hand, the irradiation of compound **1a** in solution did not show any progress of a photocyclization reaction (neither intra- nor intermolecular) and the compound decomposed due to the long-time light exposure (48 h). We assume that the presence of an anthraquinone moiety in the molecular structure of compound **1a** prevents the photocyclization reaction. Another possible explanation might be based on the shifted absorption bands of the anthracene moieties (Figure 4, see below) to lower wavelengths compared to compounds **1b** and **1c**. Despite the fact that our photoreactor can still emit the required light for the tail irradiation of compound **1a**, one can expect that the power of the lower wavelengths ( $\lambda < 450$  nm) is not so efficient. Attempts on the single-crystal-to-single-crystal photocyclization of compounds **1b** or **1c** failed due to the decomposition of the single crystals after three months of irradiation. The decyclization experiments of compounds **P1b** and **P1c** were performed in [D<sub>6</sub>]DMSO solution, where a quantitative cycloreversion was achieved in both cases around 180 °C in a reasonable time after 1.5 and 2 h, respectively (Figures S13 and S14 in the Supporting Information). The solid-state thermal decyclization of compounds **P1b** and **P1c** revealed the quantitative formation of the corresponding isomers **1b** and **1c**, respectively, after two and three days, respectively.

The structural identity of all compounds was confirmed by electrospray ionization mass spectrometry as well as by <sup>1</sup>H and <sup>13</sup>C NMR spectroscopy (Figures S1–S12 in the Supporting Infor-



**Scheme 1.** Synthesis sequence leading to the bis(tridentate) bpp ligands **1a**, **1b**, and **1c**. Conditions: i)  $\text{NaNO}_2$ ,  $\text{KI}$ ,  $\text{H}_2\text{SO}_4$ ,  $0^\circ\text{C}$ ; ii) 1)  $\text{NaBH}_4$ ,  $\text{MeOH}$ ,  $\text{RT}$ , 4 h; 2)  $\text{HCl}$ ,  $60^\circ\text{C}$ , 1 h; iii) 1)  $\text{NaBH}_4$ ,  $\text{MeOH}$ ,  $\text{RT}$ , 8 h; 2)  $\text{HCl}$ ,  $60^\circ\text{C}$ , 1 h; iv)  $\text{TIPSC}\equiv\text{CH}$ ,  $[\text{Pd}(\text{PPh}_3)_4]$ ,  $\text{CuI}$ ,  $\text{DIPA}$ ,  $\text{RT}$ ; v)  $\text{MgC}\equiv\text{CTMS}$ ,  $\text{PPh}_3$ ,  $[\text{Ni}(\text{acac})_2]$  ( $\text{acac}$  = acetylacetonate),  $\text{THF}$ ,  $60^\circ\text{C}$ ; vi)  $\text{Cs}_2\text{CO}_3$ ,  $[\text{Pd}(\text{PPh}_3)_4]$ ,  $\text{CuI}$ ,  $\text{DIPA}$ ,  $\text{THF}$ ,  $\text{RT}$ , 24 h, 4-iodo-2,6-di(1*H*-pyrazol-1-yl)pyridine; vii)  $\text{TIBAF}$ ,  $\text{THF}$ ,  $\text{RT}$ , 2 h; viii)  $[\text{Pd}(\text{PPh}_3)_4]$ ,  $\text{CuI}$ ,  $\text{DIPA}$ ,  $\text{THF}$ ,  $80^\circ\text{C}$ , 24 h, 1,8-diiodo-9,10-anthraquinone for ligand **1a**, 1,8-diiodoanthracene for ligand **1b**, and 1,8-diiodo-10-methoxyanthracene for ligand **1c**.

mation). In addition, single crystals suitable for X-ray diffraction analysis were obtained after recrystallization of the compounds from nitromethane (compound **1a**), dichloromethane/*n*-hexane (compound **P1b**) or from toluene (compounds **1c**, **P1b**, and **P1c**). The mass spectra revealed the molecular ions  $[M+H^+]$  of compounds **1a**, **1b**, **1c**, **P1b**, and **P1c** at  $m/z$  1075.30 (calcd 1075.33), 1045.32 (calcd 1045.35), 1075.36 (calcd 1075.36), 1045.32 (calcd 1045.35), and 1075.34 (calcd 1075.36), respectively. It is worth to notice that in almost all cases the  $[M+\text{Na}^+]$  ions exhibited signals of the highest stability. In particular, the mass spectrum of compound **1c** shows strong signals, which could be assigned to the molecular ions  $[2M+\text{Na}^+]$  at  $m/z$  2172.70 (calcd 2172.30) and  $[3M+\text{Na}^+]$  at  $m/z$  3248.06 (calcd 3248.06). In addition, both  $^1\text{H}$  and  $^{13}\text{C}$  NMR spectra show the expected set of signals in accordance with the molecular symmetry. Figure 2 compares the  $^1\text{H}$  NMR spectra of the final ligands before and after photoisomerization. The structural variation within all five ligands **R** does not have a significant impact on the chemical shift of the pyrazole protons, which vary in the narrow range  $\delta=7.37\text{--}7.45$  (pz3),  $6.32\text{--}6.41$  (pz4), and  $8.07\text{--}8.24$  ppm (pz5). In contrast, the pyridine protons significantly reflect the presence of the anthraquinone moiety in compound **1a** ( $\delta=7.54$  ppm; Figure S8 in the Supporting Information), whereas for the next two compounds as well as for

their isomers this signal is shifted to lower fields, that is,  $\delta=6.80\text{--}6.90$  (for compounds **1b** and **1c**) and  $6.60$  ppm (for compounds **P1b** and **P1c**). Similarly, aromatic signals of the peripheral anthracenes and the central anthraquinone units of compound **1a** acquire slightly higher values of chemical shift compared to the anthraquinone-free compounds. For both isomeric couples, that is, **1b/P1b** and **1c/P1c**, the photocyclization mainly affects the chemical shifts of the protons at the peripheral anthracene in the 9'- (9p signals around  $\delta=9.3$  ppm) and the 10'-positions (10p signals around  $\delta=7.7$  ppm), which disappeared after isomerization in favor of new signals of isomers observed around  $\delta=6.8$  (9p) and  $4.7$  ppm (10p) (Figure 2). Also, a noticeable shift to lower fields can be observed for the 9c protons of the central anthracene units. Detailed assignments of the chemical shifts are given in Figure 2.

### Crystal structures

Selected crystallographic parameters of all structurally characterized compounds are listed in Table 1. In all five cases, the single-crystal X-ray diffraction analysis confirmed the expected molecular structure of the bis(tridentate) ligands (Figure 3). For compounds **1a–1c**, two peripheral shoulders bearing the bpp moiety on the 1,8-bis(acetylene)anthracene skeleton are fur-

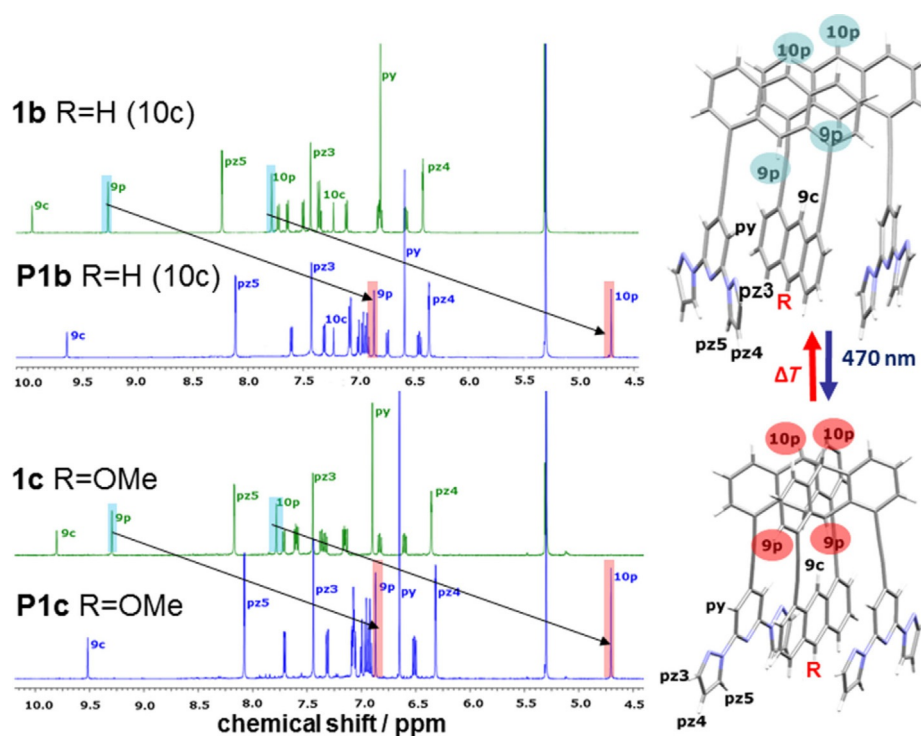


**Figure 2.**  $^1\text{H}$  NMR spectra of the compounds before (left) and after [4+4] photocyclization (right) recorded in  $\text{CD}_2\text{Cl}_2$ . Peaks labeled by “p” are attributed to peripheral anthracene rings or their photoisomers, “c”-indexed signals are attributed to the central unit (i.e., the anthraquinone moiety for compound **1a** or the anthracene moiety for compounds **1b**, **1c**, **P1b**, and **P1c**).

ther connected to the central aromatic unit (i.e., 1,8-diethynylanthraquinone for compound **1a**, 1,8-diethynylanthracene for compound **1b**, and 4,5-diethynyl-9-methoxyanthracene for compound **1c**). All three structures **1a–1c** fulfill the important requirements for a successful [4+4] photocycloaddition—the arrangement of two neighboring anthracene moieties is in the face-to-face manner with close distances of the 9'...9'' and 10'...10'' anthracene carbon atoms.

The asymmetric unit of compound **1a** (Figure 3a) contains one molecule of the ligand and one molecule of nitromethane as lattice solvent. The planes of the peripheral anthracene rings are turned to each other by an angle of  $27.4^\circ$  ( $\alpha$  angle, see Table S1 in the Supporting Information) and the distances between the 9'...9'' (C21...C52) and 10'...10'' (C53...C52) carbon atoms are 3.45 and 3.80 Å, respectively. The distances between the pyridine centroids of the bpp moieties and the central anthraquinone units are 3.78 and 4.09 Å, respectively. A detailed inspection of the non-covalent interactions revealed weak  $\pi$ - $\pi$  stacking interactions between the peripheral anthracene rings of neighboring molecules on the one site (9' and 10'' carbon atoms, C52...C53 = 3.70 Å) and the anthracene-acetylene contacts (C21...C28 = 3.63, C20...C29 = 3.68 Å) on the other site. Those two types of intermolecular contacts lead to supramolecular zigzag arrangements along the  $a$ - $b$  plane, where neighboring molecules are aligned from the opposite site parallel to each other in a head-to-head fashion, as it is displayed in Figure 3a on the right. The oxygen atoms of the lattice-included nitromethane molecule create weak contacts with neighboring hydrogen atoms of the pyrazole and anthraqui-

none moieties (the C...O contacts vary in the range 3.28–3.60 Å). The asymmetric unit of compound **1b** contains one molecule of the ligand without any presence of lattice solvent molecules. The angle between the planes of the peripheral anthracene rings is about  $9.7^\circ$  ( $\alpha$  angle, see Table S1 in the Supporting Information) and the intramolecular short contacts of the 9'...9'' (C20...C52) and 10'...10'' (C53...C21) carbon atoms are about 3.75 Å. The distances between the pyridine centroids of the bpp moiety and the central anthracene ring obeys values of 3.57 and 4.46 Å, respectively. A 1D supramolecular zigzag network was found along the  $a$ - $b$  plane, where neighboring molecules are aligned from the opposite directions in a head-to-head manner (Figure 3b, right). However, contrary to the case of compound **1a**, neighboring molecules are not strictly parallel to each other; the upper sequence of molecules is bent by a  $142^\circ$  (Figure 3b, right). Various  $\pi$ - $\pi$  interactions can be identified among the neighboring molecules; they are formed mostly between peripheral anthracene rings and acetylene moieties (Figure 3b, right). The distances of the corresponding non-covalent contacts vary in the range of 3.50–3.80 Å. The asymmetric unit of compound **1c** consists of one molecule of the ligand and one molecule of toluene as lattice solvent. The peripheral anthracene rings are arranged in face-to-face fashion; their planes are turned to each other by an angle of  $7.2^\circ$  ( $\alpha$  angle, Table S1 in the Supporting Information) with distances between the 9'...9'' (C20...C53) and 10'...10'' (C21...C54) carbon atoms of 3.63 and 3.66 Å, respectively. The distances between the pyridine centroids of the bpp moieties and the central anthracene rings are 3.50 and 3.75 Å, respec-

**Table 1.** Crystallographic data of compounds **1a**, **1b**, **1c**, **P1b**, and **P1c**.

	<b>1a</b>	<b>1b</b>	<b>1c</b>	<b>P1b</b>	<b>P1c</b>
formula	C <sub>72</sub> H <sub>38</sub> N <sub>10</sub> O <sub>2</sub> ·CH <sub>3</sub> NO <sub>2</sub>	C <sub>70</sub> H <sub>40</sub> N <sub>10</sub>	C <sub>73</sub> H <sub>42</sub> N <sub>10</sub> O·C <sub>7</sub> H <sub>8</sub>	C <sub>72</sub> H <sub>40</sub> N <sub>10</sub> ·3.5(CH <sub>2</sub> Cl <sub>2</sub> )	C <sub>73</sub> H <sub>42</sub> N <sub>10</sub> O·1.5(C <sub>7</sub> H <sub>8</sub> )
formula weight [g mol <sup>-1</sup> ]	1136.17	1045.14	1167.30	1342.38	1213.36
crystal color	red	yellow	yellow	yellow	yellow
T [K]	180(2)	180(2)	180(2)	180(2)	180(2)
λ [Å]	0.71073	0.71073	0.71073	0.71073	0.71073
crystal system	triclinic	orthorhombic	monoclinic	triclinic	monoclinic
space group	<i>P</i> $\bar{1}$	<i>Pbca</i>	<i>P2</i> <sub>1</sub> / <i>c</i>	<i>P</i> $\bar{1}$	<i>C2/c</i>
a [Å]	10.4350(10)	14.3859(4)	11.3762(8)	14.0202(7)	41.560(3)
b [Å]	15.0320(15)	19.7848(8)	37.690(3)	20.8426(10)	15.1447(6)
c [Å]	18.506(2)	36.5044(11)	14.3795(11)	23.8063(10)	21.2813(12)
α [°]	88.279(9)	90	90	68.332(3)	90
β [°]	83.385(8)	90	109.403(5)	83.982(4)	112.418(5)
γ [°]	72.276(7)	90	90	80.986(4)	90
V [Å <sup>3</sup> ]	2746.6(5)	10390.0(6)	5815.3(8)	6376.8(5)	12382.6(12)
Z	2	8	4	4	8
ρ <sub>calcd</sub> [g cm <sup>-3</sup> ]	1.374	1.336	1.333	1.398	1.302
μ (MoKα) [mm <sup>-1</sup> ]	0.088	0.081	0.081	0.366	0.079
F(000)	1176	4336	2432.0	2756	5064
crystal size [mm <sup>3</sup> ]	0.410×0.100×0.050	0.230×0.137×0.030	0.19×0.1×0.04	0.25×0.213×0.18	0.27×0.183×0.06
θ range for the data collection [°]	1.42 to 25.98	2.08 to 24.79	1.08 to 23.44	2.12 to 25.87	1.06 to 26.04
refln collected/unique	21877/10214	29426/8689	21757/9695	51675/23847	41854/11663
	[R <sub>int</sub> = 0.1173]	[R <sub>int</sub> = 0.1426]	[R <sub>int</sub> = 0.1252]	[R <sub>int</sub> = 0.0990]	[R <sub>int</sub> = 0.0631]
restraints/parameters	0/793	0/740	0/823	23/1646	0/849
refln with I > 2σ(I)	3807	3674	2930	9455	6157
final R indices [I > 2σ(I)] <sup>[a]</sup>	R1 = 0.0613 wR2 = 0.1134	R1 = 0.0544 wR2 = 0.0898	R1 = 0.0429 wR2 = 0.0492	R1 = 0.1026 wR2 = 0.2598	R1 = 0.0482 wR2 = 0.1062
R indices (all data) <sup>[b]</sup>	R1 = 0.1807 wR2 = 0.1470	R1 = 0.1655 wR2 = 0.1200	R1 = 0.1880 wR2 = 0.0693	R1 = 0.2239 wR2 = 0.3314	R1 = 0.1098 wR2 = 0.1265
GoF on F <sup>2</sup>	0.820	0.878	0.647	0.965	0.879

[a]  $R1 = \sum (F_o - F_c) / \sum (F_o)$ ;  $wR2 = \sqrt{\sum [w(F_o^2 - F_c^2)^2] / \sum [w(F_o^2)^2]}$ .

tively. One bpp moiety contains significantly twisted pyrazole rings with a torsion angle between the carbon atoms of the pyridine (3'- and 2'-position) and both nitrogen atoms of the pyrazole (1''- and 2''-position) of +153.5° (Table S1 in the Supporting Information). Such deformation is most probably a consequence of weak intermolecular hydrogen bonding between the nitrogen atom (2'-position, N1) and a pyrazole hydrogen atom of a neighboring molecule, (N1...C64 = 3.31 Å). The molecules of the ligands are aligned within the *a*-*b* plane from the opposite directions in a head-to-head fashion, however, bent to each other by an angle of 133° (Figure 3c, right). Various short contacts between the peripheral anthracene rings and the ethynyl moieties were identified among the neighboring molecules; the distances vary in the range 3.60–3.73 Å (Figure 3c, right).

The asymmetric unit of compound **P1b** consists of two ligand molecules and seven disordered molecules of the solvent dichloromethane (Figure 4a). The bond lengths formed by the photocyclization (i.e., the C21–C53, C20–C52, C93–C125, and C92–C124 bonds) are in the range of 1.61–1.65 Å and are similar as previously observed for photocyclized dianthracene moieties, see for example, references [25, 27, 28]. Two neighboring phenylene rings, which originate from the same anthracene, create angles in the range of 128–138° and the torsion angles between two opposite phenylene rings obey values in the range of 41–49° (see Table S1 and Table S1 in the Supporting Information). The distances between the pyr-

idine centroids of the bpp planes and the central anthracene rings vary in the range 3.45–3.80 Å. Neighboring molecules of the ligands are embedded within the crystal lattice in a face-to-side fashion (see Figure S15d in the Supporting Information) and do not exhibit any significant intermolecular contacts between each other. One molecule of the ligand and 1.5 molecules of toluene as lattice solvent can be found in the asymmetric unit of compound **P1c** (Figure 4b). The distances of the new bonds formed by the photocyclization (i.e., the C21–C54 and C20–C53 bonds) are about 1.60 Å; the angles between the two neighboring and opposite phenylene rings of the dianthracene moiety range in the intervals 130–137° and 43–50° (see Table S1 in the Supporting Information), respectively. The distances between the pyridine moieties and the central anthracene are 3.51 and 3.60 Å, respectively, and they are slightly shorter as compared to the isomer **1c**. The decrease of the aromaticity as well as the supramolecular arrangement of the ligands in a face-to-side manner results in the lack of intermolecular contacts within the crystal lattice.

### Absorption and emission spectroscopy

In the FTIR spectra, weak vibrational bands can be recognized around  $\tilde{\nu} = 2210$  cm<sup>-1</sup>, which are attributed to the acetylene triple bonds. Comparing the spectra of the related photoisomers, those signals show a slight increase from the bands at  $\tilde{\nu} = 2206$  (compound **1b**) and 2207 cm<sup>-1</sup> (compound **1c**) to  $\tilde{\nu} =$

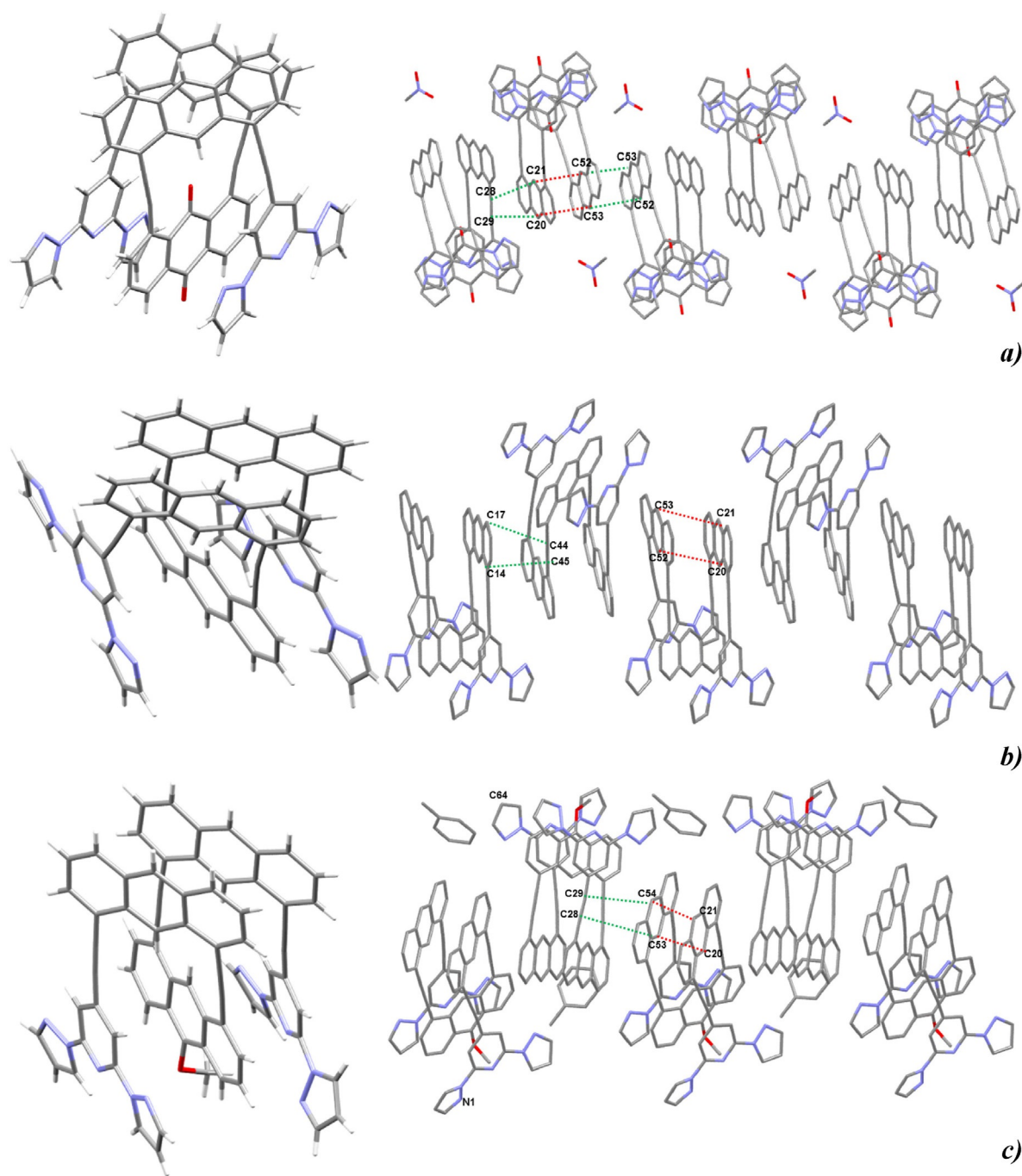


**Figure 3.** Representation of the single-crystal structures (left) and of the supramolecular arrangements within the molecular structure (right) of compounds: a) **1a**, b) **1b**, and c) **1c**. Color code: gray = carbon, white = hydrogen, blue = nitrogen, and red = oxygen. Green and red dotted lines highlight inter- and intramolecular noncovalent contacts, respectively.

2213 (compound **P1b**) and  $2214\text{ cm}^{-1}$  (compound **P1c**). The infrared spectra of the isomers revealed common vibrational bands, especially in the fingerprint region (see Figure S16 in the Supporting Information). Comparison of the anthraquinone-free compounds **1b** and **1c** with the spectrum of compound **1a** revealed small differences in the region of the stretching vibrations of the  $\text{C}_{\text{ar}}\text{-H}$  and  $\text{C}_{\text{ar}}\text{-C}_{\text{ar}}$  bonds.

The UV/Vis spectra of the bis(tridentate) ligands were measured in acetonitrile solution (Figure 5, left). All five com-

pounds show a series of vibrationally spaced bands at wavelengths of  $\lambda = 360\text{--}480\text{ nm}$  (inset in Figure 5, left), which are typical  $\pi\text{-}\pi^*$  absorptions for anthracene systems and irradiation into these bands has been reported to lead to [4+4] photocyclization. The high-energy bands are almost identical for all compounds and only slightly dependent on the substitution pattern.

The fluorescence spectra of the reported compounds were measured in acetonitrile solution ( $c \approx 10\ \mu\text{M}$ ) with  $\lambda_{\text{exc}} = 350\text{ nm}$

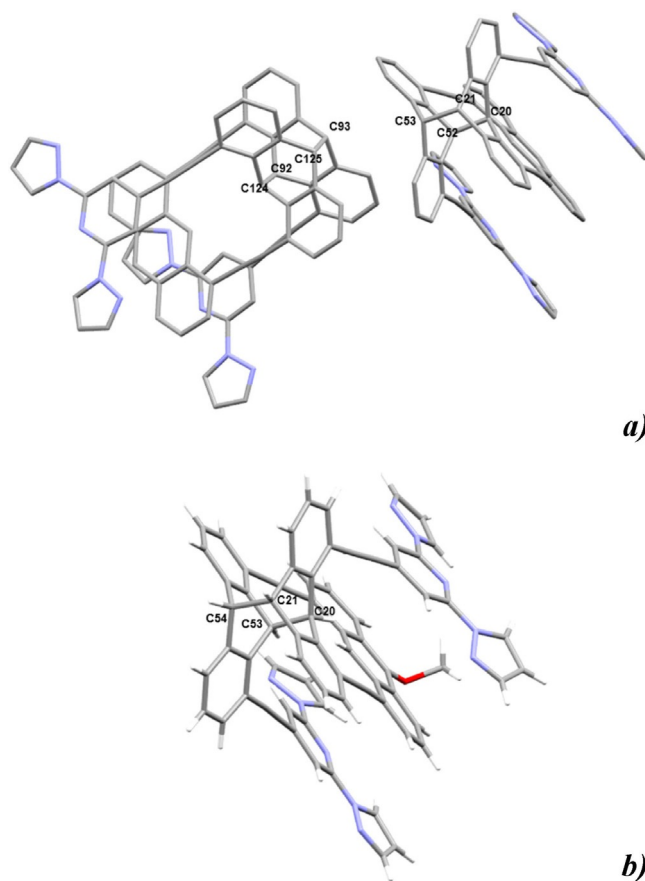


**Figure 4.** Single-crystal structures of compounds: a) **P1b**, and b) **P1c** (hydrogen atoms are omitted for the clarity). Color code: gray = carbon, white = hydrogen, blue = nitrogen, and red = oxygen.

(Figure 5, right). For compounds **1a–1c**, the maximum of the emission exhibited a slight red-shift trend to  $\lambda=475$  (compound **1a**), 480 (compound **1b**), and 492 nm (compound **1c**). The anthraquinone-free compounds also showed an additional broad shoulder centered at around  $\lambda=550$  nm for compound **1b** and  $\lambda=580$  nm for compound **1c**. A more complicated situation has been observed for the photoisomers, where the emission spectrum of compound **P1b** shows two maxima at

$\lambda=458$  and 478 nm and an additional shoulder at  $\lambda=510$  nm. Similarly, two maxima were found for compound **P1c** at  $\lambda=467$  and 492 nm and a weak and badly pronounced shoulder around  $\lambda=550$  nm was detected as well. Comparison of the spectra before and after photoisomerization revealed common emission bands at around  $\lambda=480–490$  nm and above  $\lambda=550$  nm for both couples **1b/P1b** and **1c/P1c**. Additional emission bands centered at around  $\lambda=460$  nm are attributed to the isolated phenylene–acetylene–bpp moieties of compounds **P1b** and **P1c** arising upon photoisomerization.

### Electrochemistry

a)

The redox behavior of compounds **1a**, **1b**, **1c**, **P1b**, and **P1c** was studied by cyclic voltammetry in 0.1 M TBAPF<sub>6</sub> solution in dry acetonitrile by using a Pt disk electrode as the working electrode (WE; Figure 6). It is interesting to note that the electrochemical behavior of the two corresponding isomers **1b/P1b** and **1c/P1c** is dramatically different and depends on the absence/presence of the aliphatic tricyclic moiety that arises upon [4+4] photocycloaddition. Thus, from the electrochemical point of view, the compounds can be divided in to two groups. The first group, containing compounds **1a–1c**, involves separated peripheral anthracenes in the molecular structure and their cyclic voltammograms show several broad

b)

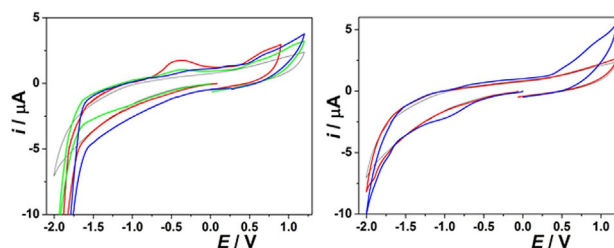


**Figure 6.** Left: cyclic voltammograms of compounds **1a** (green lines), **1b** (red lines), and **1c** (blue lines). Right: cyclic voltammograms of compounds **P1b** (red lines) and **P1c** (blue lines). The thin black lines correspond to the baseline. The measurements were performed in 0.1 M TBAPF<sub>6</sub> in dry acetonitrile. Scan rate = 128 mV s<sup>-1</sup>. A Pt disk was used as WE. The potentials are referred to the Ag|AgCl|1 M LiCl RE.

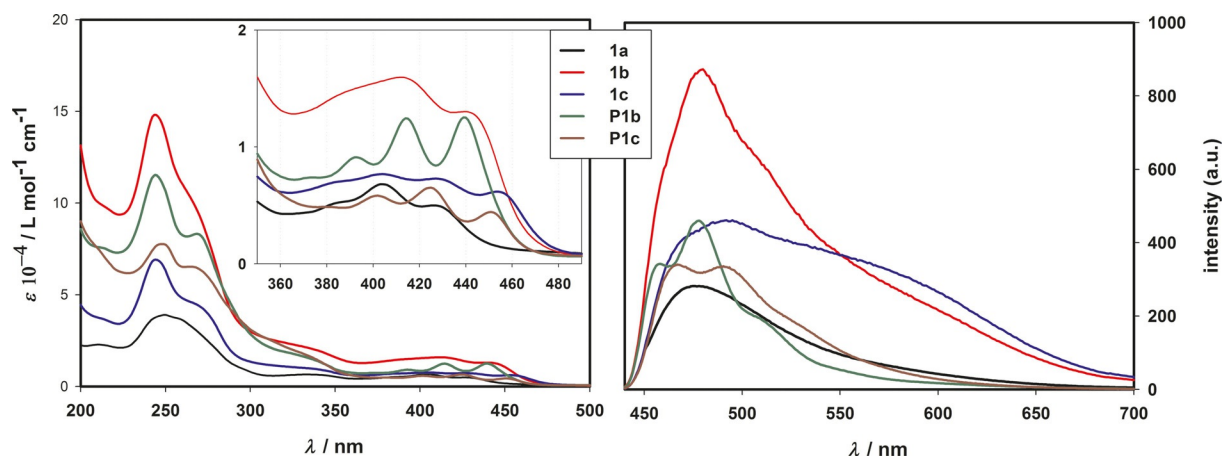


**Figure 5.** Left: UV/Vis absorption, and right: luminescence spectra of compounds **1a**, **1b**, **1c**, **P1a**, and **P1b** in acetonitrile ( $c \approx 10 \mu\text{M}$ ).

irreversible oxidation peaks (Figure 6, left), whose positions depend on the structure of the individual compound. The power of the first oxidation potential of compounds **1a** and **1b** is very similar,  $-0.370$  and  $-0.360$  V versus RE, respectively. The oxidation peak of compound **1c** is more than  $0.100$  V positively shifted. In the case of compounds **1a** and **1c**, this oxidation peak is followed by another weak peak at  $+0.125$  and  $+0.230$  V versus RE, respectively, and its power is also dependent on the structure of the "central" anthracene moiety. The second peak was absent in the case of compound **1b**. A third peak is found in the cyclic voltammograms of all three compounds at  $+0.550$  V versus RE (compound **1a**) and at  $+0.670$  V versus RE (compounds **1b** and **1c**). For all three compounds no reduction peak could be detected.

The photoisomers **P1b** and **P1c**, which contain a paranthracene moiety in the molecular structure, exhibit very different electrochemical behaviors in comparison to compounds **1b** and **1c**. In the case of compound **P1b**, neither reduction nor an oxidation peak was observed within the studied potential window (Figure 6, right, red line). The peaks found for the compound **1b** might be attributed to oxidation processes on the peripheral anthracenes or on the entire conjugated anthracene-acetylene skeleton. However, the cyclic voltammogram of compound **P1c** shows one irreversible reduction peak at  $-0.990$  V versus RE and one, badly pronounced wide oxidation peak at  $+0.880$  V versus RE. The oxidation peak is positively shifted by approximately  $0.200$  V compared to the third oxidation peak of compound **1c** (Figure 6, right, blue line). It seems that also the presence of the oxygen atoms in the "central" anthracene unit, similarly as in the case of compound **1c**, plays an important role in the electrochemical behavior of the considered compounds.

## Conclusions

In summary, we have designed and synthesized three novel organic compounds with two 2,6-bis(pyrazol-1-yl)pyridine ligand moieties on the photoisomerizable multi-anthracene backbone. The synthesis was achieved in eight steps affording the targeted compounds in 8–9% yield. Their molecular structures include peripheral anthracenes in a face-to-face arrangement, which is a necessary requirement for the observation of [4+4] photocycloaddition reactions. In two compounds, both containing three anthracene units in the organic skeleton, blue-light irradiation in solution afforded exclusive isomerization without any further di- or polymerization. The thermally driven cycloreversion takes place at above  $180^{\circ}\text{C}$  either in solution or in the solid state, and highlights the high thermal stability of related photoisomers. On the other hand, once the anthraquinone moiety was introduced to the organic backbone, the photoisomerization is completely blocked; most probably by the inhibition of the cycloaddition due to the different light absorption properties. The molecular structures of the final compounds and their related photoisomers were unambiguously confirmed by NMR spectroscopy, mass spectrometry, and by single-crystal X-ray structure analysis, and their structural, spectral, and electrochemical properties were investigated. The

herein reported target compounds are promising bis(tridentate) ligands, which might coordinate transition-metal ions and form many nuclear oligomeric clusters with regular molecular structures and outstanding physical properties. We assume that the related photoisomerizable metal complexes will exhibit a similar thermal stability as their ligands themselves and they will give access to the observation of light-induced magnetic bi-/multistability under ambient conditions; a pivotal requirement for the implementation of molecular magnetic devices in nanotechnology.

## Acknowledgement

We thank Professor Dieter Schlüter (ETH Zürich) for fruitful discussion concerning the construction of the photoreactor as well as for advices with the irradiation experiments. Grant agencies (Germany: DFG Transregio TR 88 "3 Met"; Slovakia: APVV-14-0078, APVV-14-0073, VEGA 1/0522/14, VEGA 1/0543/15 STU Grant Scheme for Support of Excellent Teams of Young Researchers, and COST Action CM1305 (ECOSTBio)) are acknowledged for financial support.

## Conflict of interest

The authors declare no conflict of interest.

**Keywords:** cycloaddition · molecular design · N ligands · photochemistry · X-ray diffraction

- [1] M. Fujita, D. Oguro, M. Miyazawa, H. Oka, K. Yamaguchi, K. Ogura, *Nature* **1995**, *378*, 469–471.
- [2] J. M. Lehn, *Science* **2002**, *295*, 2400–2403.
- [3] O. M. Yaghi, M. O'Keeffe, N. W. Ockwig, H. K. Chae, M. Eddaoudi, J. Kim, *Nature* **2003**, *423*, 705–714.
- [4] M. Ruben, U. Ziener, J. M. Lehn, V. Ksenofontov, P. Gülich, G. B. M. Vaughan, *Chem. Eur. J.* **2005**, *11*, 94–100.
- [5] *Spin Crossover in Transition Metal Compounds*, in *Top. Curr. Chem.*, Vol. 233–235 (Eds.: P. Gülich, H. A. Goodwin), Springer, Berlin/Heidelberg, **2004**.
- [6] *Spin-Crossover Materials: Properties and Applications* (Ed. M. A. Halcrow), Wiley, New York, **2013**.
- [7] E. Coronado, B. S. Tsukerblat, R. Georges, *Molecular Magnetism: From Molecular Assemblies to the Devices* (Eds.: E. Coronado, P. Delhaes, D. Gatteschi, J. S. Miller), Kluwer, Dordrecht, **1996**.
- [8] I. Nemeč, R. Marx, R. Herchel, P. Neugebauer, J. van Slageren, Z. Travnicek, *Dalton Trans.* **2015**, *44*, 15014–15021.
- [9] O. Sato, J. Tao, Y.-Z. Zhang, *Angew. Chem. Int. Ed.* **2007**, *46*, 2152–2187; *Angew. Chem.* **2007**, *119*, 2200–2236.
- [10] J.-F. Létard, P. Guionneau, O. Nguyen, J. S. Costa, S. Marcén, G. Chastanet, M. Marchivie, L. Goux-Capes, *Chem. Eur. J.* **2005**, *11*, 4582–4589.
- [11] M.-L. Boillot, C. Roux, J.-P. Audiere, A. Dausse, J. Zarembowitch, *Inorg. Chem.* **1996**, *35*, 3975–3980.
- [12] M.-L. Boillot, S. Pillet, A. Tissot, E. Riviere, N. Claiser, C. Lecomte, *Inorg. Chem.* **2009**, *48*, 4729–4736.
- [13] A. Bannwarth, S. O. Schmidt, G. Peters, F. D. Sönnichsen, W. Thimm, R. Herges, F. Tuzcek, *Eur. J. Inorg. Chem.* **2012**, 2776–2783.
- [14] A. Sour, M.-L. Boillot, E. Riviere, P. Lesot, *Eur. J. Inorg. Chem.* **1999**, 2117–2119.
- [15] M.-L. Boillot, S. Chantraine, J. Zarembowitch, J.-Y. Lallemand, J. Prunet, *New J. Chem.* **1999**, *23*, 179–184.

- [16] M. Castellano, J. Ferrando-Soria, E. Pardo, M. Julve, F. Lloret, C. Mathoniere, J. Pasán, C. Ruiz-Pérez, L. Canadillas-Delgado, R. Ruiz-García, J. Cano, *Chem. Commun.* **2011**, 47, 11035–10983.
- [17] Y. Ishida, A. S. Achalkumar, S. Kato, Y. Kai, A. Misawa, Y. Hayashi, K. Yamada, Y. Matsuoka, M. Shiro, K. Saigo, *J. Am. Chem. Soc.* **2010**, 132, 17435–17466.
- [18] C. Yang, C. Ke, W. Liang, G. Fukuhara, T. Mori, Y. Liu, Y. Inoue, *J. Am. Chem. Soc.* **2011**, 133, 13786–13789.
- [19] E. R. Thapaliya, B. Captain, F. M. Raymo, *J. Org. Chem.* **2014**, 79, 3973–3981.
- [20] H.-D. Becker, *Chem. Rev.* **1993**, 93, 145–172.
- [21] H. Bouas-Laurent, A. Castellán, J.-P. Desvergne, R. Lapouyade, *Chem. Soc. Rev.* **2000**, 29, 43–55.
- [22] H. Bouas-Laurent, A. Castellán, J.-P. Desvergne, R. Lapouyade, *Chem. Soc. Rev.* **2001**, 30, 248–263.
- [23] M. Servalli, L. Gyr, J. Sakamoto, A. D. Schlüter, *Eur. J. Org. Chem.* **2015**, 4519–4523.
- [24] M. Li, F. G. Klärner, J. Sakamoto, A. D. Schlüter, *Chem. Eur. J.* **2013**, 19, 13348–13354.
- [25] M. Li, A. D. Schlüter, J. Sakamoto, *J. Am. Chem. Soc.* **2012**, 134, 11721–11725.
- [26] P. Kissel, R. Erni, W. B. Schweizer, M. D. Rossell, B. T. King, T. Bauer, S. Götzinger, A. D. Schlüter, J. Sakamoto, *Nat. Chem.* **2012**, 4, 287–291.
- [27] M. J. Kory, M. Wörle, T. Weber, P. Payamyar, S. W. van de Poll, J. Dshemuchadse, N. Trapp, A. D. Schlüter, *Nat. Chem.* **2014**, 6, 779–784.
- [28] P. Kissel, D. J. Murray, W. J. Wulfstange, V. J. Catalano, B. T. King, *Nat. Chem.* **2014**, 6, 774–778.
- [29] I. Šalitraš, O. Fuhr, R. Kruk, J. Pavlik, L. Pogány, B. Schäfer, M. Tatarko, R. Boča, W. Linert, M. Ruben, *Eur. J. Inorg. Chem.* **2013**, 1049–1057.
- [30] I. Šalitraš, L. Pogány, M. Ruben, R. Boča, W. Linert, *Dalton Trans.* **2014**, 43, 16584–16587.
- [31] I. Šalitraš, N. T. Madhu, R. Boča, J. Pavlik, M. Ruben, *Monatsh. Chem.* **2009**, 140, 695–733.
- [32] N. T. Madhu, I. Salitros, F. Schramm, S. Klyatskaya, O. Fuhr, M. Ruben, *C. R. Chim.* **2008**, 11, 1166–1174.
- [33] M. A. Halcrow, *Coord. Chem. Rev.* **2009**, 253, 2493–2514.
- [34] V. A. Money, J. S. Costa, S. Marcén, G. Chastanet, J. Elhaik, M. A. Halcrow, J. A. K. Howard, J.-F. Létard, *Chem. Phys. Lett.* **2004**, 391, 273–277.
- [35] J. M. Lovell, J. A. Joule, *Synth. Commun.* **1997**, 27, 1209–1212.
- [36] X. Bu, L. W. Deady, G. J. Finlay, B. C. Baguley, W. A. Denny, *J. Med. Chem.* **2001**, 44, 2004–2014.
- [37] I. Salitros, O. Fuhr, A. Eichhofer, R. Kruk, J. Pavlik, L. Dihan, R. Boca, M. Ruben, *Dalton Trans.* **2012**, 41, 5163–5171.
- [38] O. V. Dolomanov, L. J. Bourhis, R. J. Gildea, J. A. K. Howard, H. Puschmann, *J. Appl. Crystallogr.* **2009**, 42, 339–341.
- [39] G. M. Sheldrick, *Acta Crystallogr. Sect. A* **2008**, 64, 112–122.
- [40] G. M. Sheldrick, *Acta Crystallogr. Sect. C* **2015**, 71, 3–8.
- [41] U. S. Schubert, H. Hofmeier, G. R. Newkome, *Modern Terpyridine Chemistry*, Wiley-VCH, Weinheim, **2006**.
- [42] A. Wild, A. Winter, F. Schlütter, U. S. Schubert, *Chem. Soc. Rev.* **2011**, 40, 1459–1511.
- [43] M. Ruben, E. Breuning, J.-M. Lehn, V. Ksenofontov, F. Renz, P. Gütllich, G. B. M. Vaughan, *Chem. Eur. J.* **2003**, 9, 4422–4429.
- [44] E. Breuning, M. Ruben, J.-M. Lehn, F. Renz, Y. Garcia, V. Ksenofontov, P. Gütllich, E. Wegelius, K. Rissanen, *Angew. Chem. Int. Ed.* **2000**, 39, 2504–2507; *Angew. Chem.* **2000**, 112, 2563–2566.
- [45] T. Matsumoto, G. N. Newton, T. Shiga, S. Hayami, Y. Matsui, H. Okamoto, R. Kumai, Y. Murakami, H. Oshio, *Nat. Commun.* **2014**, 5, 3865–3868.
- [46] B. Schäfer, J.-F. Greisch, I. Faus, T. Bodenstern, I. Šalitraš, O. Fuhr, K. Fink, V. Schünemann, M. M. Kappes, M. Ruben, *Angew. Chem. Int. Ed.* **2016**, 55, 10881–10885; *Angew. Chem.* **2016**, 128, 11040–11044.
- [47] M. Goichi, K. Segawa, S. Suzuki, S. Toyota, *Synthesis* **2005**, 2116–2119.

Manuscript received: February 21, 2017

Accepted manuscript online: May 10, 2017

Version of record online: July 4, 2017